LA-UR 93-1382

Los Alamos National Laboratory is operated by the University of California for the United States Department of Energy under contract W-7405-ENG-36

LA-UR--93-1382

DE93 012682

TITLE:

MHD Simulation of Deuterium-Fiber-Initiated Z-Pinches with Two-Fluid Effects

AUTHOR(S):

Peter Sheehey and Irvin R. Lindemuth

SUBMITTED TO

Proceedings of Third International Conference on Dense Z-Pinches, Imperial College, London, England, April 20-23, 1993

Los Alamos National Laboratory
Los Alamos, New Mexico 87545

MHD SIMULATION OF DEUTERIUM-FIBER-INITIATED Z-PINCHES WITH TWO-FLUID EFFECTS

Peter Sheehey
Department of Physics, University of California
Los Angeles, California 90024 USA

Irvin R. Lindemuth
Los Alamos National Laboratory
Los Alamos, New Mexico 87545 USA

ABSTRACT

Two-dimensional "cold-start" resistive MHD computations of formation and evolution of deuterium-fiber-initiated Z-pinches [1,2] have been extended to include separate ion and electron energy equations and finite-Larmor-radius ordered terms[3,4]. In the Ohm's Law (magnetic field evolution) equation, Hall and diamagnetic pressure terms have been added, and corresponding terms have been added to the energy equations. Comparison is made of the results of these computations with previous computations and with experiment[5].

INTRODUCTION

Deuterium-fiber-initiated Z-pinch experiments, with current peaks up to about 600 kA, reported very long-lived, compact plasmas showing little indication of disruption by m=0 "sausage" or m=1 "kink" instabilities[6-8]. Second-generation machines[5,9,10] have been designed to reach the Pease-Braginskii current (about 1.4 MA for deuterium)[11-13], in the hope that fusion conditions could be approached, if the earlier observed "anomalous stability" were to hold. Discharges at greater than half Pease-Braginskii current (700-900 kA)[5,9], however, have shown stronger indication of expansion and m=0 instability growth. We have done extensive computational modeling[1,2] of low- and high-current deuterium-fiber-initiated experiments on the Los Alamos machines HDZP-I[7,8] and -II[5,8]. Here we present some results of the extension of our computational model to include: 1) separate ion and electron energy equations; 2) Hall and diamagnetic pressure terms in the magnetic field evolution equation.

First, a brief discussion of the scope of the computational problem: For a significant fraction of its lifetime, a fiber-initiated Z-pinch plasma meets classical requirements for description as a magnetohydrodynamic (MHD) fluid (e.g., ion-ion collision time $\ll$ ion thermal transit time)[2,14]. Furthermore, the consistent (but so far unexplained) observation that three-dimensional behavior (e.g., growth of m=1 "kink" instabilities) is virtually absent in such experiments (diagnostic images are highly symmetric about the axis)[5,9] gives us some confidence in the results of MHD simulation in only two dimensions. This is fortunate, because the inclusion of vital experimental and physics details discussed below would at present make full 3-d simulation prohibitively expensive.

Linear ideal MHD stability theory for a Z-pinch plasma in general predicts instability to "sausage" (m = 0) and "kink" (m = 1) modes[15]. However, the

growth rate of such instabilities is dependent on radial pressure profiles of the plasma; indeed, "Kadomtsev" profiles exist which are m=0 stable. Any actual experiment is likely to move through several non-ideal regimes (e.g., resistive MHD, Hall MHD), as density, temperature, etc., vary during the discharge; nonlinear effects, as well, are likely to be encountered.

Therefore, it is highly desirable to simulate such experiments starting from time zero (zero current, frozen fiber) if possible, in order for realistic plasma profiles to form and develop linearly/nonlinearly, as they will. Energy terms such as thermal conduction, Joule heating and radiation are clearly going to be important. The plasma column must be free to develop as if in vacuum, without the influence of an unrealistically confining or insufficiently resolved grid.

METHOD

The computations reported here are an extension of previous one-[16] and two-dimensional[1,2] deuterium-fiber-initiated Z-pinch modeling. We have used an alternating-direction-implicit numerical method, utilizing Newton-Raphson-like iteration to deal with nonlinear quantities, to solve the two-dimensional (r,z) MHD equations for mass density, specific internal energy, azimuthal magnetic field, and perpendicular velocity (v_r, v_z)[17]:

$$\frac{\partial \rho}{\partial t} + \nabla \cdot (\rho \vec{v}) = 0$$

$$\frac{\partial (\rho \vec{v})}{\partial t} + \nabla \cdot (\rho \vec{v} \vec{v}) + \nabla p - \vec{J} \times \vec{B} = 0$$

$$\frac{\partial (\rho \epsilon)}{\partial t} + \nabla \cdot (\rho \vec{v} \epsilon) + p \nabla \cdot \vec{v} - \nabla \cdot (\kappa_\perp \nabla T) - \eta \vec{J}^2 + Q_{rad} = 0$$

$$\frac{\partial \vec{B}}{\partial t} + \nabla \times (-\vec{v} \times \vec{B} + \frac{\eta}{\mu_0} \nabla \times \vec{B}) = 0$$

where ρ is mass density, $\vec{v}$ is velocity, $\vec{B}$ is magnetic field, $\vec{J} (= \nabla \times \vec{B}/\mu_0)$ is electrical current density, ϵ is specific internal energy, p is pressure, T is temperature, Q_{rad} is radiative energy loss, η is electrical resistivity, and $\kappa_\perp$ is (perpendicular) thermal conductivity. To obtain the equation of state (specific energy and pressure), the ionization level, the radiative energy loss, and the resistivity, we use the Los Alamos SESAME[18] tabulated atomic data base computer library. Thermal conductivity follows Braginskii[19].

For two temperature runs, the above total energy equation is replaced by separate ion and electron energy equations:

$$\frac{\partial (\rho \epsilon_e)}{\partial t} + \nabla \cdot (\rho \vec{v} \epsilon_e) + p_e \nabla \cdot \vec{v} - \nabla \cdot (\kappa_e \nabla T_e) - \eta \vec{J}^2 + Q_{rad} + Q_{ei} = 0$$

$$\frac{\partial (\rho \epsilon_i)}{\partial t} + \nabla \cdot (\rho \vec{v} \epsilon_i) + p_i \nabla \cdot \vec{v} - \nabla \cdot (\kappa_i \nabla T_i) - Q_{shock} - Q_{ei} = 0$$

where ϵ_α, p_α, T_α, and $\kappa_{\perp\alpha}$ refer to the appropriate ion or electron quantities, Q_{ei} is the electron-ion energy equilibration term, and Q_{shock} is an ion shock-heating term. Because of problems encountered with the SESAME electron and ion equations of state at very low temperatures, it was necessary to use ideal gas equations of state; in one-temperature runs, this was found to have no major effect on the results, compared to SESAME one-temperature runs. Resistivity, radiation loss, and ionization level were still taken from SESAME.

Hall MHD runs replace the above magnetic field evolution equation with:

$$\frac{\partial \vec{B}}{\partial t} + \nabla \times (-\vec{v} \times \vec{B} + \frac{\eta}{\mu_0} \nabla \times \vec{B} + \frac{1}{en_e}(\vec{J} \times \vec{B} - \nabla p_e)) = 0$$

where n_e is electron number density and e is the charge magnitude of the electron. It was found that the Hall ($\nabla \times (\vec{J} \times \vec{B}/n_e)$) term acted as a strong nonlinear magnetic field convection operator, destabilizing the usual time- and space-centered alternating-direction-implicit algorithm. A stable adaptation of the algorithm was developed by treating the effective convective velocity (proportional to $\vec{J}/n_e$) explicitly and using a donor-cell (but still time-centered) treatment of the $\vec{B}$ convected. This two-dimensional Hall MHD program was successfully tested on the Kingsep-Mokhov-Chukbar magnetic penetration problem discussed by Mason[20]. To preserve total energy conservation, a term complementary to the diamagnetic pressure term was added to the total energy equation: $p_e \nabla \cdot (-\vec{J}/en_e)$. Hall MHD runs to date have not yet been done with the two-temperature model, although we expect to do this shortly.

Actual experimental current vs. time values provide the boundary condition for magnetic field at the outer radial wall. "Cold-start" initial conditions are a solid, cryogenic deuterium fiber, surrounded to about twice the fiber radius by a low density, "warm" halo plasma (density $10^{-3}\times$solid, temperature 1 eV), which provides an initial current conduction path. Our computed results are insensitive to the details of this halo plasma after a short-lived (10 nsec) transient, because of the small mass involved relative to the fiber-generated plasma. The surrounding vacuum is simulated by a cold, very low density region extending out to a zero-temperature, electrically insulating wall. The early fiber-ablation stage of the discharge necessitates relatively fine radial grid spacing, but because this stage can be followed by an explosive expansion of the heating plasma, the radial grid is checked at each timestep, and adjusted so that the outer boundary is always at least 150% of the radius within which 95% of the total axial current is contained.

Radial grids of $\sim$100 points, more finely spaced near the axis to better resolve the fiber/plasma column, cover a radius as small as 1 mm, but ultimately as large as several cm, if rapid expansion is followed. In the original, single temperature MHD runs, axial sections from 2 cm down to 0.25 mm, covered with uniformly spaced axial grids of 31 to 62 points, were used, respectively capable of resolving the largest (X ray "bends") and smallest (shadowgram "spicules") features observed in any of the experiments. Although the smallest, most finely

resolved grids did show fine-scale instability growth starting earlier than the larger grids, saturation of shorter wavelengths resulted in larger grids ultimately showing faster expansion. Hence the timing of instability development and expansion varied by as much as 20 nsec for different grid sizes, but this is comparable to experimental timing uncertainties (e.g., the relation between driving voltage, current, and diagnostic images in time). Extended model runs to date have only been done with 1 mm and 1 cm, 31-point axial grids; more complete coverage of potential instability scales is planned.

RESULTS

Our single-temperature MHD simulations of the Los Alamos experiments HDZP-I (250 kA peak at 125 nsec)[1,2,7] and HDZP-II (750 kA peak at 100 nsec)[2,5,8] showed early development of m=0 instabilities in the plasma corona, which carries most of the current as the fiber ablates. These instabilities, and associated expansion of the plasma column in terms of mass or current, were not well reflected in the shadowgram images of the early experiment (Fig. 1(a-d)). The later, higher-current experiment HDZP-II reached complete ionization of the fiber much more quickly, at which point full nonlinear instability development led to intense nonuniform heating and rapid expansion of the plasma column (Fig. 2(a-d)). The agreement between simulation-generated diagnostic images (shadowgrams and interferograms), and actual experimental data, is strong. The variations we have modeled to date in fiber thickness, current ramp, and plasma initiation show some differences in timing of the instability-driven expansion, but expansion soon after complete ionization always appears.

As temperatures rise and density drops (e.g., in narrow m=0 "necks"), the appropriateness of the collisional fluid model (requiring ion-ion collision time $\ll$ ion thermal transit time)[2,14] breaks down. Even before this, however, is lost the more stringent requirement for ion-electron energy equilibration:

$$\frac{\left(\frac{m_i}{m_e}\right)^{\frac{1}{2}} v_{th}\tau_{ii}}{a} = \frac{\left(\frac{m_i}{m_e}\right)^{\frac{1}{2}} \tau_{ii}}{\tau_{th}} \ll 1.$$

Simulation results with two energy equations were fundamentally similar to those with only one temperature. An interesting detail was noted: Early in the discharge (and always in 1 d simulations), electron temperature, driven by ohmic heating, remained above or equal to ion temperature. When the 2 d runs began to show drastic nonlinear instability development (such as in Fig. 2), shock heating of ions associated with steep velocity gradients became dominant, causing ion temperatures to significantly exceed electron temperatures, both peak (Fig. 3(a)) and average (Fig 3(b)). Hence an instability heating mechanism may be further contributing to plasma column expansion.

The Hall and diamagnetic pressure terms are usually ordered out of the fluid model on the basis of small relative Larmor radius[14]. Haines and others[3,4] have noted that these terms may indeed not be small in the case of the Z pinch, with its field null on axis; as well, there may be regions in the low density coronal

plasmas generally seen in our simulations (particularly in areas of high electron density gradient) where these terms will be important. In our simulations with these terms, we do see small-wavelength instabilities appear at the edge of the plasma corona, before any instabilities were seen in the simple MHD runs (Fig. 4(a-b)). However, the ultimate pattern of instability-driven heating and expansion is still seen in the Hall runs done to date. There is a strong convection of magnetic field in the axial (current) direction, leading to a visible depletion of field at the cathode and build-up at the anode. Although something like this might actually occur at the true experimental axial boundaries, it is probably unrealistic at computational "mirror" boundaries only 1 mm apart. We may implement periodic axial boundary conditions, in order to allow a more realistic field flow through the computational axial section taken, in addition to doing a variety of axial section lengths (computing an actual 5-cm axial section could be done, but would require a coarse axial grid which would potentially suppress small-wavelength instabilities).

There are other fluid terms of finite-Larmor-radius order: the transverse thermoelectric (Nernst and Ettinghausen) effects, an energy convection by (electron) current term, and terms in the viscous stress tensor. We hope to implement the first two of these soon, although as we found with the Hall term, new physics may entail new numerical difficulties of unknown severity. Within the collisional fluid regime treated here, we argue that viscous stress will be negligible relative to pressure gradient effects[14]. Such an argument may not hold in the "collisionless MHD" regime, in which experiments proposed by Haines and others[10,21] are purported to dwell. A further extension of the present work would be into the "collisionless MHD" regime, perhaps following an experimental plasma as it passes from collisional to collisionless.

A fiber-initiated Z-pinch plasma may provide an appropriately heated and magnetized plasma for implosion inside a heavy liner to fusion conditions, in a "magnetized target fusion" scheme. In addition, implosion of a hollow, initially solid deuterium cylinder by a fiber-Z-pinch-style fast current ramp may be a route to fusion that avoids the instability problems seen in the fiber Z-pinches simulated here. We are employing the computational tools developed for the work reported here in the evaluation of these related concepts.

CONCLUSIONS

Detailed two-dimensional MHD simulations of deuterium fiber Z-pinches have shown good agreement to the Los Alamos experiments HDZP-I and HDZP-II. Late in low current and early in higher current experiments, when the fiber has become fully ionized, $m = 0$ instabilities develop rapidly, and drive intense nonuniform heating and rapid expansion of the plasma column, dropping densities orders of magnitude below the high densities desired for fusion conditions. We believe the "cold start" approach taken here is vital to the realistic simulation of such experiments, due to the close tie between plasma profiles and stability. Inclusion of the finite Larmor radius effects and two temperature model presented here does not change these basic conclusions. If an experiment

is to reach potentially stabilizing conditions in a "collisionless MHD" or other regime, it would appear desirable to avoid the dangerously unstable collisional MHD area explored in our simulations. Fiber-initiated Z-pinches may have potential in magnetized target fusion and related concepts.

ACKNOWLEDGMENTS

We would like to acknowledge the assistance of the HDZP-I/II experimental group: R. Lovberg, D. Scudder, J. Shlachter, et al; and stimulating discussions with N. Bobrova, J. Chittenden, P. Choi, M. Coppins, J. Dawson, H. Etlicher, M. Haines, M. Liberman, R. Mason, A. Robson, P. Sasorov, and J. Sethian.

REFERENCES

1. I. R. Lindemuth, Phys. Rev. Lett. **65**, 179 (1990).
2. P. Sheehey, J. Hammel, I. Lindemuth, R. Lovberg, R. Riley Jr., D. Scudder, J. Shlachter, Phys. Fluids B **4**, 3698 (1992).
3. M. G. Haines, J. Phys. D **11**, 1709 (1978).
4. M. Coppins, D. J. Bond, and M. G. Haines, Phys. Fluids **27**, 2886 (1984).
5. D. W. Scudder, J. S. Shlachter, J. E. Hammel, F. Venneri, R. Chrien, R. Lovberg, R. Riley, in Physics of Alternative Magnetic Confinement Schemes, Proceedings of the Workshop Held at Varenna, Italy, 1990 ed. S. Ortolani and E. Sindoni (SIF, Bologna, 1991), p. 519.
6. J. D. Sethian, A. E. Robson, K. A. Gerber, and A. W. DeSilva, Phys. Rev. Lett. **59**, 892 (1987); **59**, 1790(E) (1987).
7. J. Hammel and D. Scudder, in Proceedings of the Fourteenth European Conference on Controlled Fusion and Plasma Physics, Madrid, Spain, 87 F. Engelmann and J. L. Alvarez Rivas (EPS, Petit-Lancy, Switzerland, 1987), p. 450.
8. J. E. Hammel, in Dense Z-Pinches, ed. by N. R. Pereira, J. Davis, and N. Rostoker (American Institute of Physics, New York, 1989), p. 303.
9. J. Sethian, A. Robson, K. Gerber, and A. DeSilva, in Physics of Alternative Magnetic Confinement Schemes (Ref. 5), p. 511.
10. M. Haines, in Physics of Alternative Magnetic Confinement Schemes (Ref. 5), p. 277.
11. R. S. Pease, Proc. Phys. Soc. B **70**, 11 (1957).
12. S. I. Braginskii, Sov. Phys. JETP **6**, 494 (1958).
13. N. R. Pereira, Phys. Fluids B **2**, 677 (1990).
14. J. Freidberg, Ideal Magnetohydrodynamics (Plenum Press,New York,1987) Ch. 2.
15. B. B. Kadomtsev, in Reviews of Plasma Physics, edited by M. A. Leontovich (Consultants Bureau, New York, 1966), Vol. 2, p. 165.
16. I. R. Lindemuth, G. H. McCall and R. A. Nebel, Phys. Rev. Lett. **62**, 264 (1989).
17. I. R. Lindemuth, UC Lawrence Livermore Laboratory Report UCRL 52492 (1979).
18. Los Alamos National Laboratory Report LA-10160-MS, ed. by K. S. Holian

(1984).
19. S. I. Braginskii, in Reviews of Plasma Physics, edited by M. A. Leontovich (Consultants Bureau, New York, 1965), Vol. 1, p. 205.
20. R. Mason, P. Auer, R. Sudan, B. Oliver, C. Seyler, and J. Greenly, Phys. Fluids B **5**, 1 (1993).
21. M. Haines and M. Coppins, Phys. Rev. Lett. **66**, 1462 (1991).

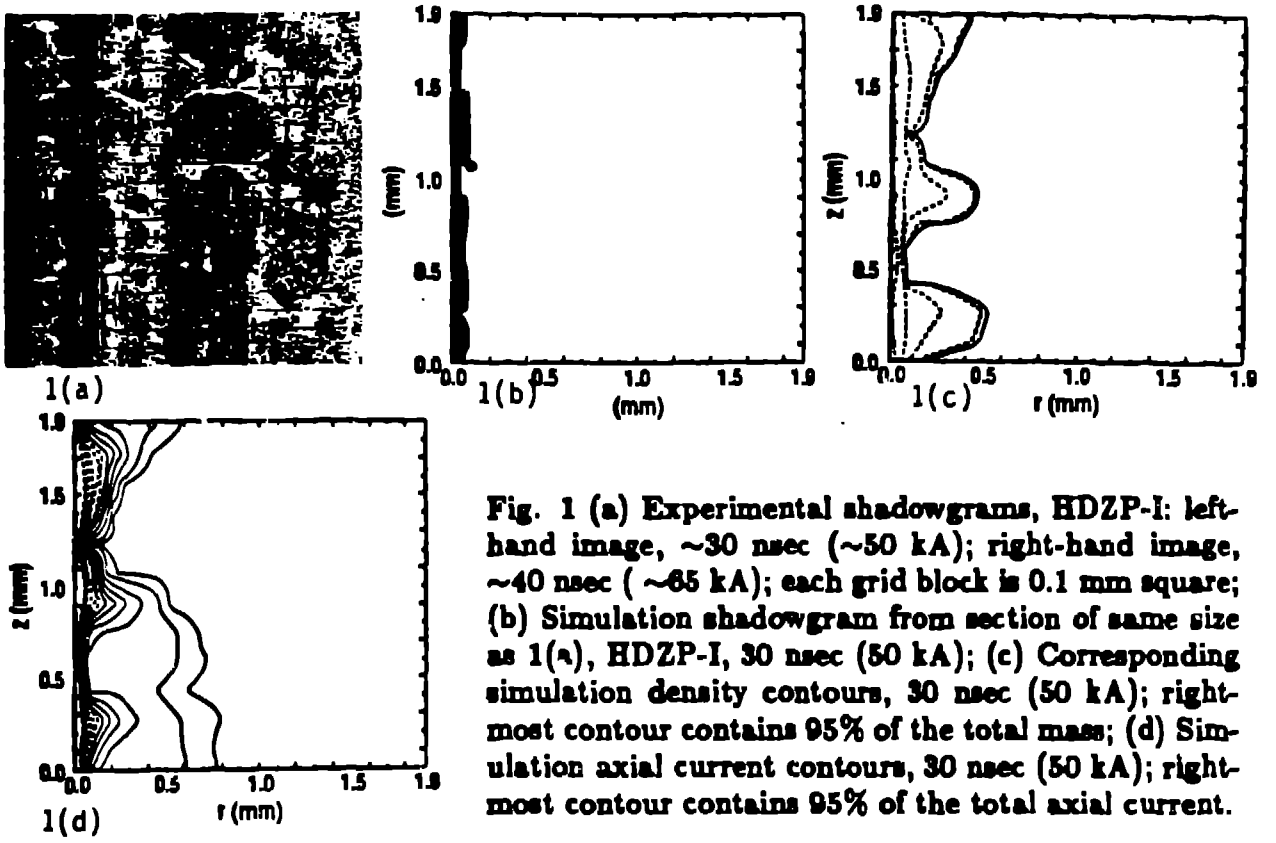

Fig. 1 (a) Experimental shadowgrams, HDZP-I: left-hand image, ~30 nsec (~50 kA); right-hand image, ~40 nsec (~65 kA); each grid block is 0.1 mm square; (b) Simulation shadowgram from section of same size as 1(a), HDZP-I, 30 nsec (50 kA); (c) Corresponding simulation density contours, 30 nsec (50 kA); rightmost contour contains 95% of the total mass; (d) Simulation axial current contours, 30 nsec (50 kA); rightmost contour contains 95% of the total axial current.

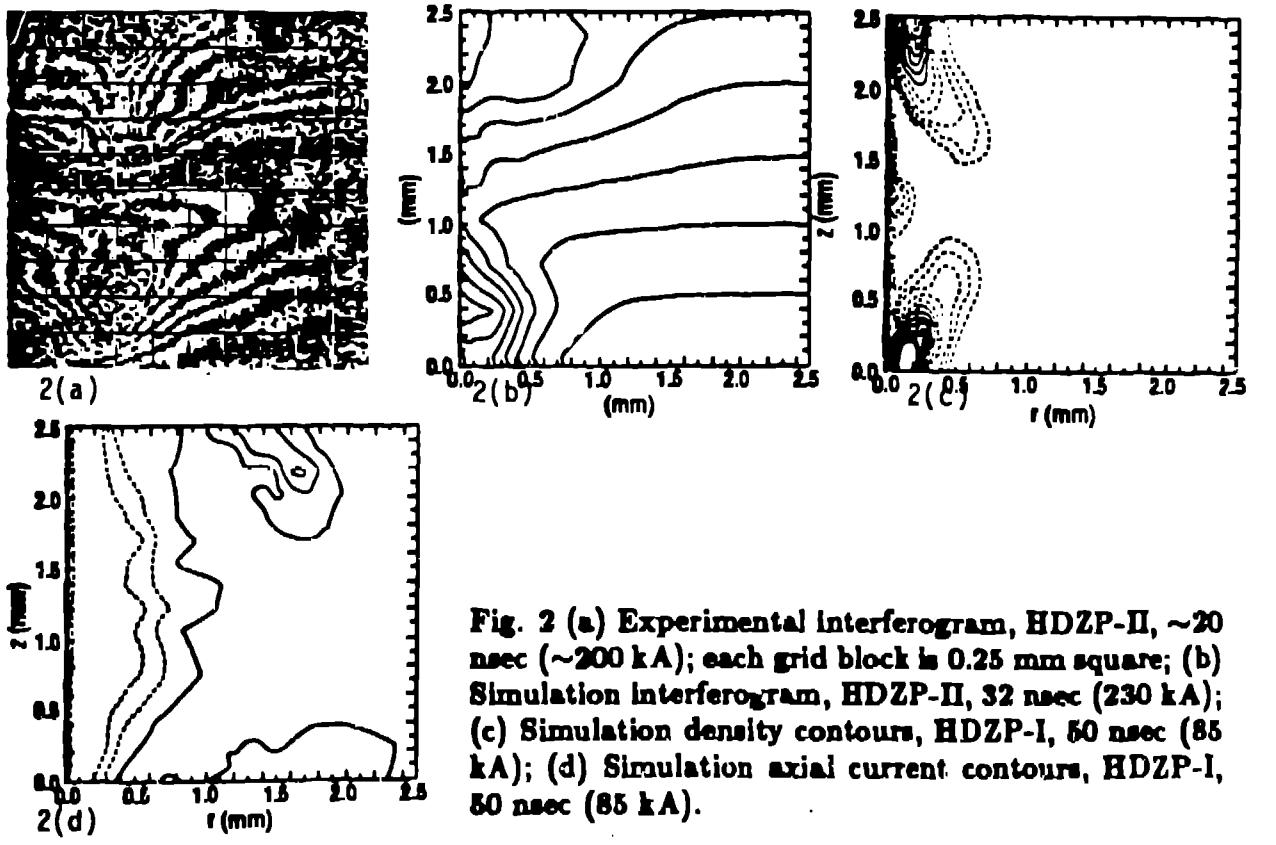

Fig. 2 (a) Experimental interferogram, HDZP-II, ~20 nsec (~200 kA); each grid block is 0.25 mm square; (b) Simulation interferogram, HDZP-II, 32 nsec (230 kA); (c) Simulation density contours, HDZP-I, 50 nsec (85 kA); (d) Simulation axial current contours, HDZP-I, 50 nsec (85 kA).

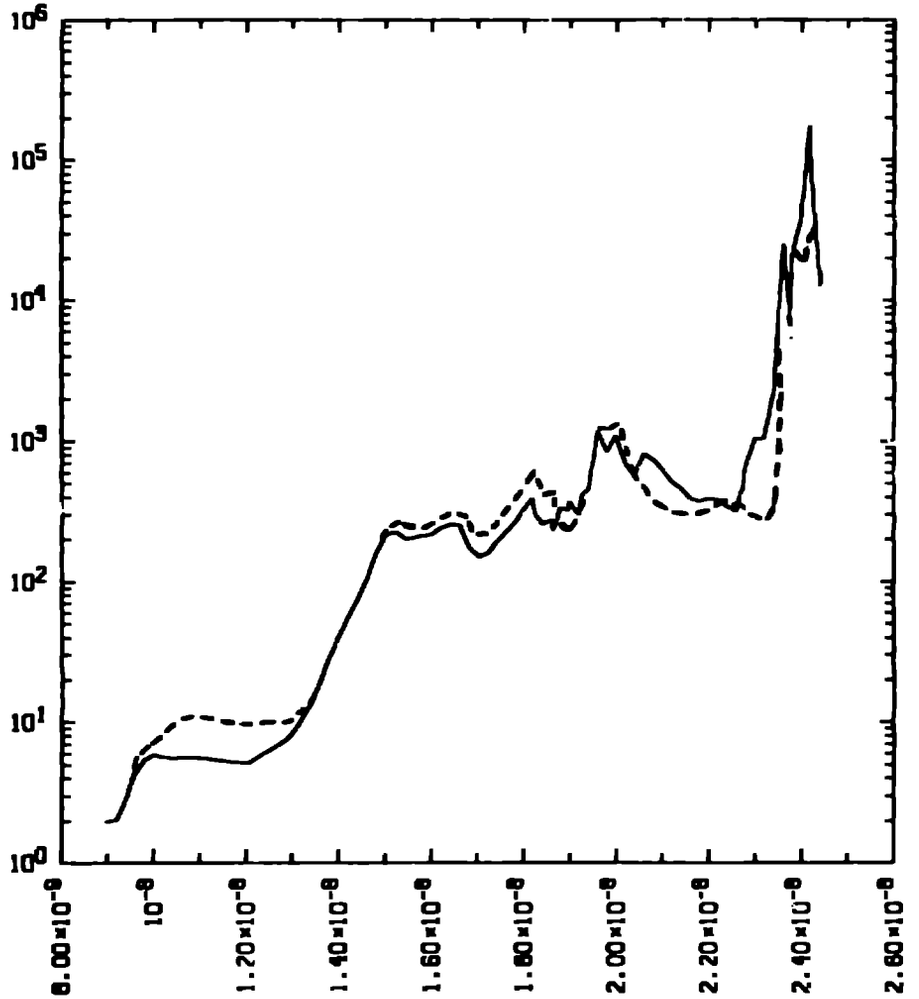

— MAX. ION TEMP. VS T Z2T77

- MAX ELEC TEMP

FIG. 3. MAXIMUM ION TEMPERATURE VS. TIME (SOLID)
MAXIMUM ELECTRON TEMP. VS. TIME (DOTTED).

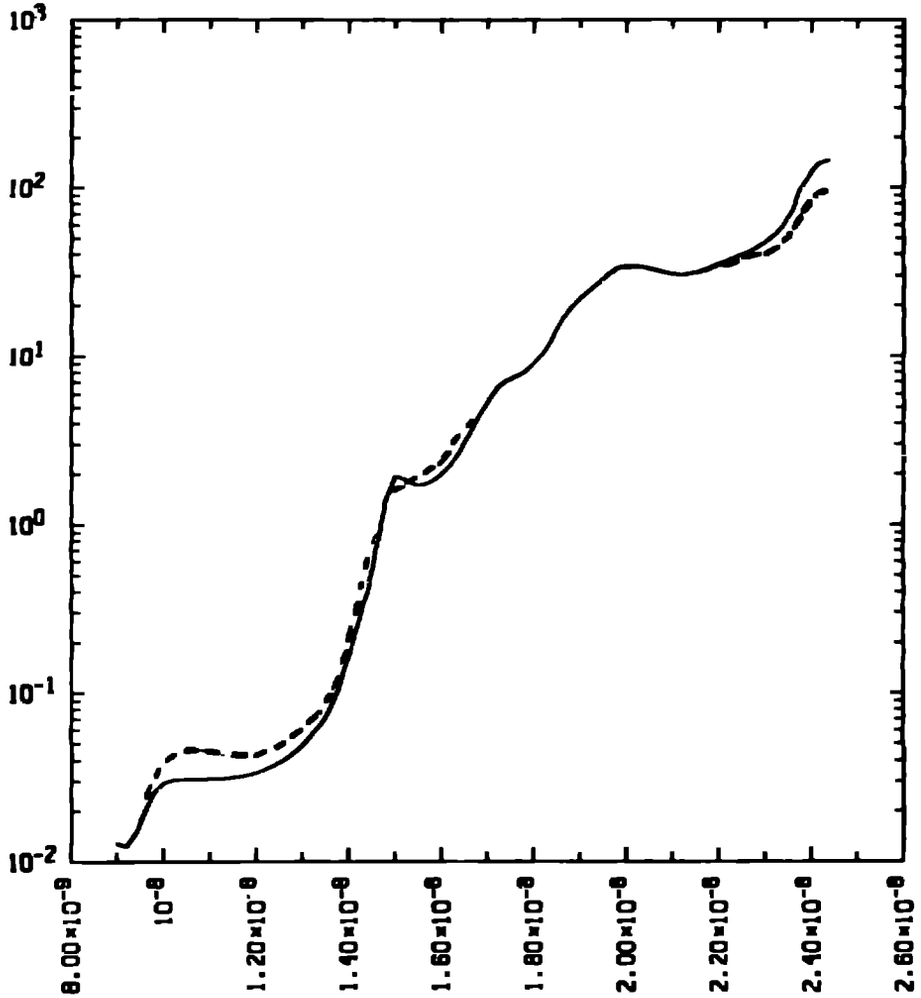

AVE. ION TEMP. VS T Z2T77

A.E. ELEC. TEMP

FIG. : AVERAGE ION TEMP. VS. TIME (SOLID)
AVERAGE ELECTRON TEMP. VS. TIME (DOTTED

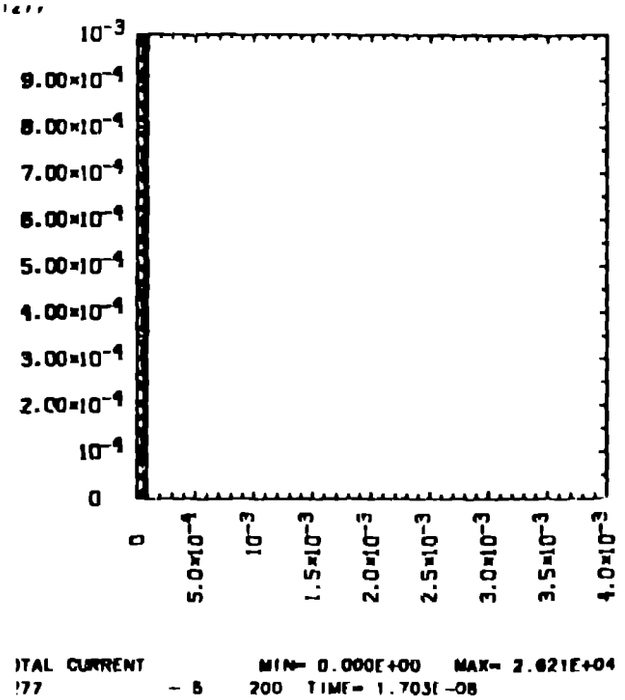

FIG. 4(A) AXIAL CURRENT PROFILES, 9 nSEC (30KA), MHD SIMULATION

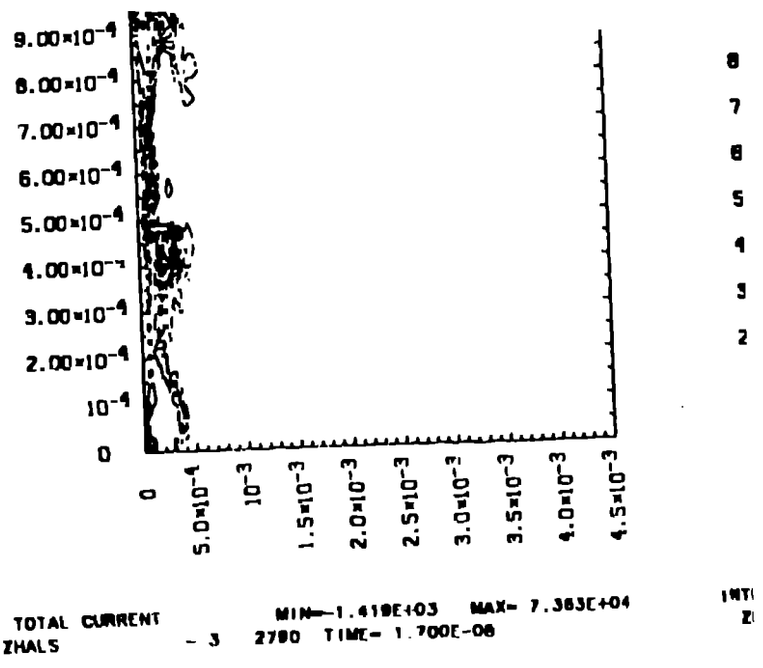

FIG 4(B) AXIAL CURRENT PROFILES, 9 nSEC (30KA), HALL MHD SIMULATION